Bifurcation and hysteresis in a nonlinear transport model on network motifs

Hajime Koike [*]
School of Computing, Tokyo Institute of Technology, Yokohama 226-8502, Japan

Hideki Takayasu
Sony Computer Science Laboratories, Tokyo 141-0022, Japan
and School of Computing, Tokyo Institute of Technology, Yokohama 226-8502, Japan

Misako Takayasu [†]
School of Computing, Tokyo Institute of Technology, Yokohama 226-8502, Japan

(Received 12 September 2023; accepted 1 December 2023; published 16 January 2024)

Nonlinear transport has been observed in many real systems, such as international trade, business transactions, human movement, and urban traffic. To understand the fundamental properties of transport in such systems, several models have been proposed in the past few years. These models exhibit complex behavior due to the interplay between nonlinearity and the underlying network topology. We studied a transport equation on three-body network motifs both numerically and analytically, and we found bifurcation on two motifs and hysteresis of a model on one motif. These three motifs show different bifurcation points. The first two motifs have a branching node, i.e., a node with outdegree 2, and the third motif is a fully connected bidirectional triangle. In particular, the hysteresis on the bidirectional triangle is not predictable from the linear stability analysis on the uniform stationary solution. The analysis based on the self-consistency equation of the parameter u [see Eq. (6) for the precise definition] measuring the ratio between sizes on two nodes reveals the following: The bifurcation on the first two motifs is due to supercritical pitchfork bifurcation. The difference between these two motifs comes from the existence of bidirectional edges. The hysteresis on the third motif is due to the combination of the saddle-node and transcritical bifurcation. Our results imply that the nonlinear transport model exhibits nontrivial behavior even in minimal settings and that the bifurcation on large-scale networks becomes far more complex and unpredictable from the underlying network structure.

DOI: 10.1103/PhysRevResearch.6.013059

I. INTRODUCTION

Nonlinear transport has been found in many phenomena in the world. As a typical example of nonlinear transport, nonlinear effects have been observed in world trade [1] and population movement among countries and cities [2–4], where the larger the size of the flow target, the larger the flow rate approximated by a nontrivial power-law relation, which is called the gravity law. In addition, in recent studies on complex systems, the number of observed nonlinear flows has continued to expand to various scales of human-flow systems [5–8], transportation systems [9,10], international trade [1,11], and even business-to-business transactions [12].

Despite the fact that such nonlinear transport has been known for a long time, theoretical issues, such as the stability of the stationary state associated with the nonlinearity of transport, have not been sufficiently investigated until recently. In the past few years, there has been a rapid increase in interest in these fundamental properties, and several models generalizing the classical random walk with constant transition probability have been proposed. Specifically, there have been several models that generalize the usual discrete-time nonlinear random walk with transition probabilities depending on the current state [13–16], and the continuous-time nonlinear transport model with injection and dissipation, on which flux between two sites depends on the target state [17,18]. It has been found that these models exhibit complex and diverse behaviors, such as bifurcations [13,17,18], quasiperiodic solutions [14], chaos [15], localized patterns [16], and aggregation phenomena [19] due to nonlinearity, even under relatively few degrees of freedom and regular grid structures. Therefore, complex behaviors of solutions in these models of nonlinear transport imply that predictive control is fundamentally difficult, even on a regular grid structure with few degrees of freedom. The behavior of these models on complex networks for describing real phenomena is expected to be even more difficult to evaluate and awaits further study.

In this article, we numerically and analytically investigate the behavior of the three-body system in which nonlinearity

[*]koike.h.af@m.titech.ac.jp
[†]Corresponding author: takayasu.m.aa@m.titech.ac.jp

is modeled by a power function. Although 3 is the minimum degree of freedom that exhibits nontrivial behavior, we show that the bifurcation points and types of bifurcation phenomena change depending on the underlying network structure. We found hysteresis in the bidirectional triangle, i.e., a three-body fully connected graph, and show that the type of branching changes in response to changes in the structure by adding edges in the three systems out of all 13 network motifs with three nodes. These results suggest that we expect more complex bifurcations as the number of degrees of freedom is increased and that it will be difficult to determine the values of the bifurcation points. However, we hope that our results can demonstrate that only a few degrees of freedom can explain the qualitative behavior observed in large-scale networks [20].

The remainder of this paper is organized as follows. Section II presents the model definition, numerical results on three-body motifs, and linear stability analysis; Sec. III presents the bifurcation analysis with self-consistent equations; and finally, Sec. IV presents our conclusions.

II. MODEL AND NUMERICAL RESULTS

In this article, we study the following time evolution of size variables x_j for each node $j = 1, 2, \ldots, N$ on the directed network with N nodes:

$$\frac{dx_j}{dt} = \sum_i \frac{A_{ij}x_j^\gamma}{\sum_k A_{ik}x_k^\gamma}x_i - (1+\nu)x_j + 1, \tag{1}$$

where A_{ij} is the adjacency matrix of the network, i.e., $A_{ij} = 1$ if there exists a directed edge from i to j and $A_{ij} = 0$ otherwise; $\gamma \geqslant 0$ is a nonlinearity parameter; and $\nu > 0$ is a parameter determining the average value of the stationary solution of Eq. (1):

$$\langle x \rangle = \frac{1}{N}\sum_{j=1}^{N} x_j = \frac{1}{\nu}, \tag{2}$$

which can be understood as the conservation law of the total amount. Equation (1) is obtained as the transport equation on the network with uniform linear dissipation with coefficient ν and uniform constant injection based on the flux, with the functional form modeled by

$$f_{ij} \propto A_{ij}x_i x_j^\gamma. \tag{3}$$

The interaction (3) includes the law of mass action [21] if $\gamma = 1$. Equation (3) includes a typical type of interaction called gravity law which can be found in other examples such as international trade between countries [1], business transaction between companies [12], and human movement [3]. In this context, the size variable x represents the annual gross domestic product, annual sales, and population of cities, respectively. A previous study reports that Zipf's law of the distribution of annual sales of companies can be replicated using Eq. (1) on the Japanese business network by setting $\gamma = 0.33$ and $\nu = 0.1$ [17].

The role of γ in model (1) is to control the degrees of preferences, which node i sends more flux to node j for higher x_j. The case when γ is zero corresponds to ordinary diffusion, while the case with positive γ corresponds to nonlinear transport under which flux from two nodes depends on the size of the target node.

This model has previously been shown to exhibit bifurcation by controlling γ for fixed ν on many networks [17,18], including large-scale networks like the Japanese business network. Since the discovery of bifurcation in the Japanese business network, the transition point γ_c has been investigated. It was previously found that γ_c may depend on the underlying network structure, and γ_c of the Japanese business network is approximately 0.9 (when $\nu = 0.1$) [17]. Moreover, a regular ring structure has been proposed as a network replicating the transition point of the Japanese business network [18]. According to the ubiquity of the nonlinear flow in the real systems, it may be possible to observe this bifurcation phenomena empirically.

In the recent literature on complex systems, the behavior of the dynamics on the large-size network has been a main focus [22–24]. Here, we instead study the model on the three-body directed connected motifs, or so-called network motifs [25,26], to explore the behavior of the minimal-size systems. We study the bifurcation on all 13 network motifs with three nodes. We found only three out of all motifs exhibit bifurcation. We found discontinuous bifurcations both with and without hysteresis on two classes of three-body motifs.

To study the model behavior, we focused on the behavior of the stationary solution $\mathbf{x}(\gamma)$ depending on γ for fixed ν. For fixed perturbation $\delta\mathbf{x}$, we introduce the following protocol, as shown in Fig. 1(b). We simulate the consecutive process of calculating $\mathbf{x}^{(u)}(\gamma)$ for $\gamma_0 \leqslant \gamma \leqslant \gamma_1$ and $\mathbf{x}^{(d)}(\gamma)$ for $\gamma_1 \geqslant \gamma \geqslant \gamma_0$, where we start calculation of $\mathbf{x}^{(u)}(\gamma_0)$ and then calculate $\mathbf{x}^{(u)}(\gamma)$ using the initial value $\mathbf{x}^{(u)}(\gamma - \Delta\gamma) + \delta\mathbf{x}$ iteratively from $\gamma = \gamma_0$ to reach $\gamma = \gamma_1$. We set $\mathbf{x}^{(d)}(\gamma_1) = \mathbf{x}^{(u)}(\gamma_1)$, and after that we then calculate $\mathbf{x}^{(d)}(\gamma)$ using the initial value $\mathbf{x}^{(d)}(\gamma + \Delta\gamma) + \delta\mathbf{x}$ iteratively from $\gamma = \gamma_1$ to $\gamma = \gamma_0$ in turn. We fix $\nu = 0.01$ and calculate the stationary solution of Eq. (1) by the Euler method using the time step $\Delta t = 1$. We set perturbation $\delta\mathbf{x}$ to two types. For the first case, $\delta\mathbf{x} = (0, 1, 0)$, and for the second, $\delta\mathbf{x} = (1, 1, 0)$. The perturbation is needed to avoid the realization of the unstable solution. We set the condition that the time evolution is convergent if the average over vertices of the absolute difference between the present and previous steps is less than 10^{-8}. We set $\gamma_0 = 0.0$, $\gamma_1 = 5.0$, and $\Delta\gamma = 10^{-3}$.

We performed numerical simulation on all 13 network motifs and found only three classes; i.e., motifs 1, 8, and 13 in Fig. 1(c) exhibit bifurcation. We show the results obtained for three classes in Figs. 2(a)–2(d). We confirmed that the stationary solution was the same for motifs 1–12, while that of motif 13 was different for these two perturbations and independent of the magnitude of the perturbations as well. We show the numerical results of all 13 motifs in Appendix.

In Fig. 2(a), it can be observed from the bifurcation diagram of motif 1 that a supercritical pitchfork bifurcation occurs. The bifurcation point is $\gamma = 3$, which is understood to be caused by the symmetry breaking between the green and blue nodes. Even if the symmetry of the these nodes is broken by the bifurcation, the difference between them is within a certain range. In Fig. 2(b), the bifurcation diagram for motif 8 shows a supercritical pitchfork bifurcation like in motif 1. In this case, the bifurcation point is 1, but it is difficult

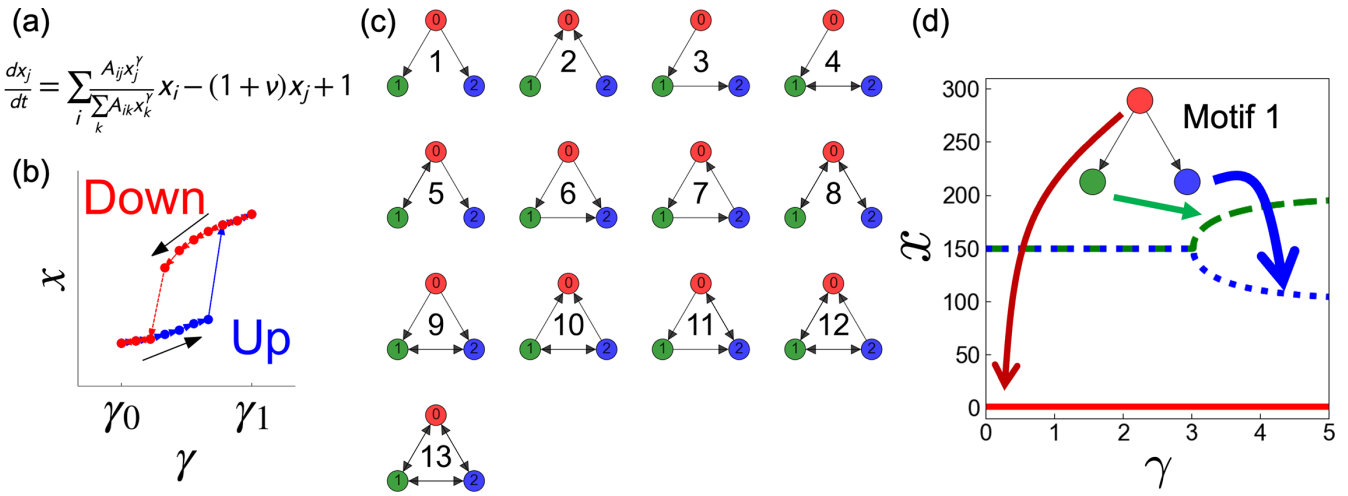

FIG. 1. Overview of the numerical experiment on all 13 network motifs with three nodes. (a) The model we consider. The fraction appearing in the first term on the right-hand side determines the proportion of inflow coming from the neighborhood of node j. We study the stationary solution of this model throughout this article. We control the parameter γ and examine whether nontrivial behavior happens to the stationary solution. (b) The numerical simulation protocol. Initially, we set $\gamma = \gamma_0$ and calculate the stationary solution. Then, starting from the stationary solution for $\gamma - \Delta\gamma$, we add the fixed perturbation $\delta\mathbf{x}$ and then calculate the stationary solution $\mathbf{x}(\gamma)$ of the equation displayed in panel (a). We iterate this process up to $\gamma = \gamma_1$, and then we add perturbation $\delta\mathbf{x}$ and calculate the stationary solution $\mathbf{x}(\gamma - \Delta\gamma)$ to reach the starting $\gamma = \gamma_0$. (c) All 13 network motifs with three nodes. For each motif, we consider the process described in panel (b) and obtain stationary solutions. (d) The resulting bifurcation diagram with underlying motif. The horizontal axis is the control parameter γ, and the vertical axis is the value of the stationary solution x. The red, green, and blue nodes are nodes 0, 1, and 2 in panel (c), respectively. The solid red line, dashed green line, and dotted blue line correspond to the values of the stationary solution at the red, green, and blue nodes, respectively. For illustration, we show the bifurcation diagram for motif 1. We show the diagrams that exhibit bifurcation for motifs 1, 8, and 13 in Fig. 2, and we show the results for all 13 motifs in Appendix. Motif 1 was found to exhibit supercritical pitchfork bifurcation as a result.

to determine from the numerical results alone whether the stationary solution at the bifurcation has the same continuity as motif 1. Intuitively, the reason why the bifurcation point of motif 8 is smaller than that of motif 1 is that the symmetry between the blue and green nodes is more easily broken due to the transfer from the blue node to the green node caused by the bifurcation. This is because there exists a positive feedback mechanism only on motif 8, not on motif 1. Figures 2(c) and 2(d) show bifurcation diagrams obtained for the same motif 13. The difference between the two figures is the perturbation: Fig. 2(c) is the case where $\delta\mathbf{x} = (0, 1, 0)$, i.e., only the green node is perturbed, while Fig. 2(d) is the case where $\delta\mathbf{x} = (1, 1, 0)$, i.e., the red and green nodes are perturbed. In Fig. 2(c), the bifurcation appears to be continuous, but

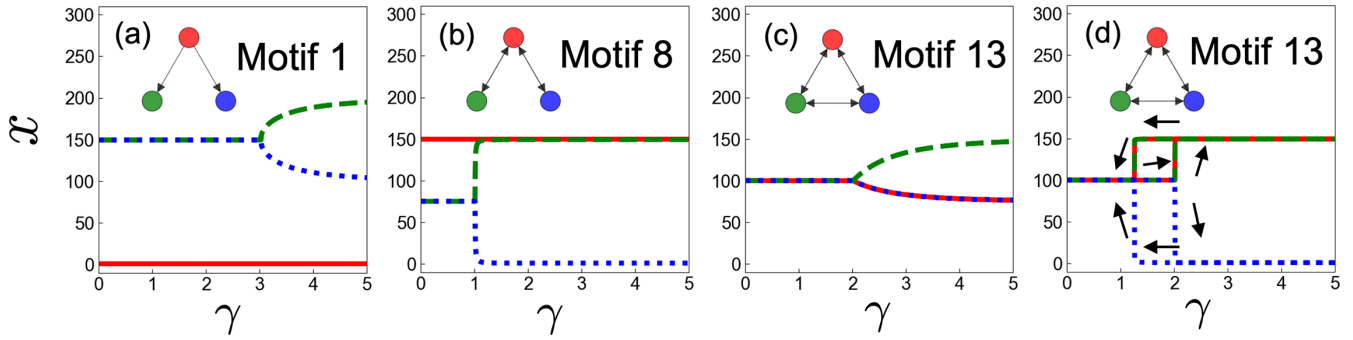

FIG. 2. Bifurcation diagrams of motifs 1, 8, and 13. For each panel (a)–(d), the horizontal axis is the control parameter γ, and the vertical axis is the value of the stationary solution x. The colors of nodes in the motifs correspond to the colors of the curves. We fix $\nu = 0.01$ for simulation. We have confirmed that the existence of bifurcation still holds for smaller ν values. (a) The bifurcation diagram of motif 1. The bifurcation point is approximately 3, which is confirmed by Eq. (4a). The value of the red node does not change throughout the protocol. The type of bifurcation is the supercritical pitchfork bifurcation due to the symmetry of green and blue nodes breaking. (b) The bifurcation diagram of motif 8. The bifurcation point is approximately 1, which is consistent with Eq. (4b). Again, the value of the red node does not change throughout the protocol. The type of bifurcation is the supercritical pitchfork bifurcation for finite ν, and the slope goes to infinity at the zero-dissipation limit $\nu \to 0$. (c) The bifurcation diagram of motif 13 with positive perturbation added on the green node. (d) The bifurcation diagrams of motif 13 with positive perturbation added on the red and green nodes. The hysteresis loop is obtained on motif 13, i.e., a bidirectional triangle. The hysteresis in $\gamma_c^{(d)} = 1.26 \leqslant \gamma \leqslant \gamma_c^{(u)} = 2.01$ is present.

in Fig. 2(d), a discontinuous bifurcation with hysteresis is observed. As the bifurcation in Fig. 2(c) is different from the case with $\mathbb{Z}_2$ symmetry, it is unclear from the numerical calculations whether it is a pitchfork bifurcation or not.

On these motifs, the stationary solution at $\gamma \leqslant \gamma_c$ can be analytically derived. By linear stability analysis of the stationary solution, one can obtain

$$\text{motif 1: } \gamma_c^{(1)} = 3 + 2\nu, \tag{4a}$$

$$\text{motif 8: } \gamma_c^{(8)} = 1 + 2\frac{(2+\nu)\nu}{3+\nu}, \tag{4b}$$

$$\text{motif 13: } \gamma_c^{(13u)} = 2 + \frac{4}{3}\nu. \tag{4c}$$

These formulas prove the existence of bifurcation at finite γ values, even at the zero-dissipation limit $\nu \to 0$. The bifurcation points of the three motifs are different. This demonstrates the difficulty of estimating the bifurcation point for large-size systems from the underlying network structure.

The eigenvectors corresponding to the leading eigenvalues of the Jacobian are

$$\text{motif 1: } v_1 = (0, 1, -1), \tag{5a}$$

$$\text{motif 8: } v_8 = (0, 1, -1), \tag{5b}$$

$$\text{motif 13 : } \begin{cases} v_{13}^{(1)} = (0, 1, -1), \\ v_{13}^{(2)} = (1, 0, -1). \end{cases} \tag{5c}$$

Equations (5a)–(5c) show that while motifs 1 and 8 have only one leading eigenmode, motif 13 has two. Motifs 1 and 8 exhibit an essentially unique localized stationary solution at $\gamma > \gamma_c$ up to symmetry, while motif 13 exhibits two distinct types of localized stationary solution. This is partly because motifs 1 and 8 have only one eigenmode corresponding to the largest eigenvalue in the vicinity of bifurcation, but motif 13 has two eigenmodes. Two distinct linear combinations of these two eigenmodes may correspond to the two different localized solutions after bifurcation in Figs. 2(c) and 2(d).

III. BIFURCATION ANALYSIS BY SELF-CONSISTENCY EQUATION

In this section, we present the results of the bifurcation analysis by self-consistency equation for motifs 1, 8, and 13. Here, we introduce the parameter u to measure the degree of deviation between the sizes of nodes 1 and 2:

$$u = \ln \frac{x_2}{x_1}. \tag{6}$$

$u = 0$ corresponds to the uniform state with $x_1 = x_2$, and $u \neq 0$ indicates the localized state. We analyze the behavior of u to understand the behavior of the stationary solution in the vicinity of the bifurcation. In the following, we show the result of bifurcation analysis for motifs 1, 8, and 13.

A. Motifs 1 and 8

Here, we derive the self-consistency equation of u on motifs 1 and 8 as

$$u = \phi(u, \gamma, \nu) \equiv \ln \frac{(x_0+1)e^{\gamma u} + 1}{x_0 + 1 + e^{\gamma u}}. \tag{7}$$

To obtain Eq. (7), we start with the stationary solution on motif 1:

$$(1+\nu)x_0 = 1, \tag{8a}$$

$$\nu x_1 = \frac{1}{1 + \left(\frac{x_2}{x_1}\right)^{\gamma}} x_0 + 1, \tag{8b}$$

$$\nu x_2 = \frac{1}{1 + \left(\frac{x_2}{x_1}\right)^{-\gamma}} x_0 + 1. \tag{8c}$$

By taking the ratio between Eqs. (8b) and (8c), we get Eq. (7). Equation (8a) determines the stationary solution x_0 of node 0. In the case of motif 8, by taking the second and third equations of the stationary solution,

$$(1+\nu)x_0 = x_1 + x_2 + 1, \tag{9a}$$

$$(1+\nu)x_1 = \frac{1}{1 + \left(\frac{x_2}{x_1}\right)^{\gamma}} x_0 + 1, \tag{9b}$$

$$(1+\nu)x_2 = \frac{1}{1 + \left(\frac{x_2}{x_1}\right)^{-\gamma}} x_0 + 1, \tag{9c}$$

we obtain the same self-consistency equation (7) as for motif 1. The difference between motifs 1 and 8 is the value of x_0 obtained by solving Eqs. (8) and (9), respectively:

$$\text{motif 1: } x_0 = \frac{1}{1+\nu}, \tag{10a}$$

$$\text{motif 8: } x_0 = \frac{3+\nu}{\nu(2+\nu)}. \tag{10b}$$

As usual in the analysis of the self-consistency equation of the order parameter in the context of mean-field theory, the bifurcation point is determined by

$$\left.\frac{\partial \phi}{\partial u}\right|_{u=0} = \frac{\gamma x_0}{x_0 + 2} = 1. \tag{11}$$

Thus, we have

$$\gamma_c = 1 + \frac{2}{x_0}. \tag{12}$$

The bifurcation points of motifs 1 and 8 from Eq. (12) combined with Eqs. (10a) and (10b) coincide with the point obtained by linear stability analysis in Eqs. (4a) and (4b).

The behavior of ϕ is described in Figs. 3(b) and 3(c) on motif 1 and in Figs. 4(b) and 4(c) on motif 8 at fixed $\nu = 10^{-2}$. According to Figs. 3(c) and 4(c), ϕ on motif 1 does not change for different ν, while ϕ on motif 8 changes significantly. The shape of the ϕ curve differs at the bifurcation point between motif 1 [Fig. 3(b)] and motif 8 [Fig. 4(b)]. Hence, the asymptotic behavior of x_0 at $\nu \to 0$ is key to identifying the type of bifurcation on motifs 1 and 8. In the case of motif 1, the bifurcation is continuous even at $\nu \to 0$ because x_0 is finite. Meanwhile, in the case of motif 8, the bifurcation becomes discontinuous at $\nu \to 0$ even if it is continuous at finite $\nu > 0$. Indeed, the localized solution is finite only if $\nu > 0$.

The behavior of the solution of the self-consistency equation after bifurcation by changing ν is different according to

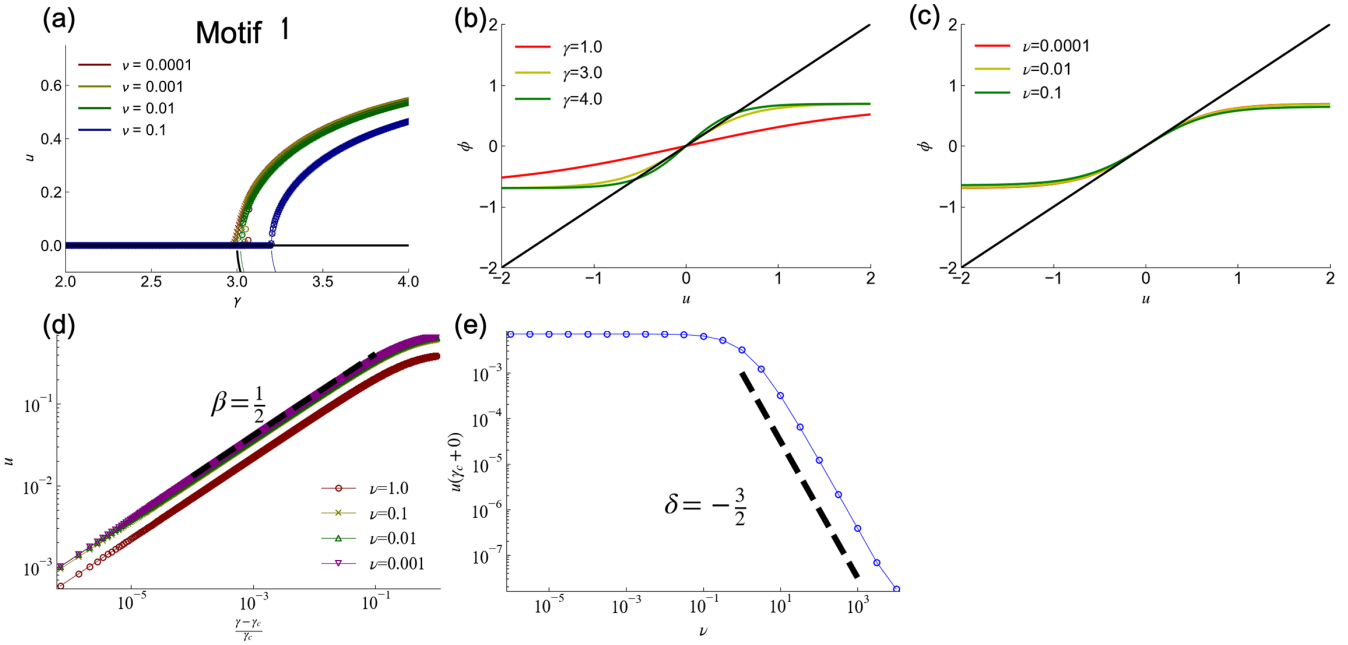

FIG. 3. Bifurcation analysis on motif 1 based on the self-consistency equation (7). (a) The solution of Eq. (7) for $\nu = 10^{-4}$ (red), 10^{-3} (yellow), 10^{-2} (green), and 10^{-1} (blue). Points are the results obtained by numerically calculated stationary solution. Lines are the results based on Eq. (7). The black line indicates the solution of the self-consistency equation (7) at $\nu \to 0$. (b) The curves of the right-hand side ϕ of Eq. (7) at $\nu = 10^{-2}$ for $\gamma = 1.0$ (red), 3.0 (yellow), and 4.0 (green). (c) The curves of the right-hand side ϕ of Eq. (7) at $\gamma = \gamma_c = 3 + 2\nu$ for $\nu = 10^{-4}$ (red), 10^{-2} (yellow), and 10^{-1} (green). (d) The scaling relationship of Eq. (13a) obtained by solving Eq. (7) numerically. The black line indicates the theoretical prediction of Eq. (18). (e) The scaling relationship of Eq. (13b) obtained by solving Eq. (7) numerically. The black line indicates the theoretical prediction of Eq. (20).

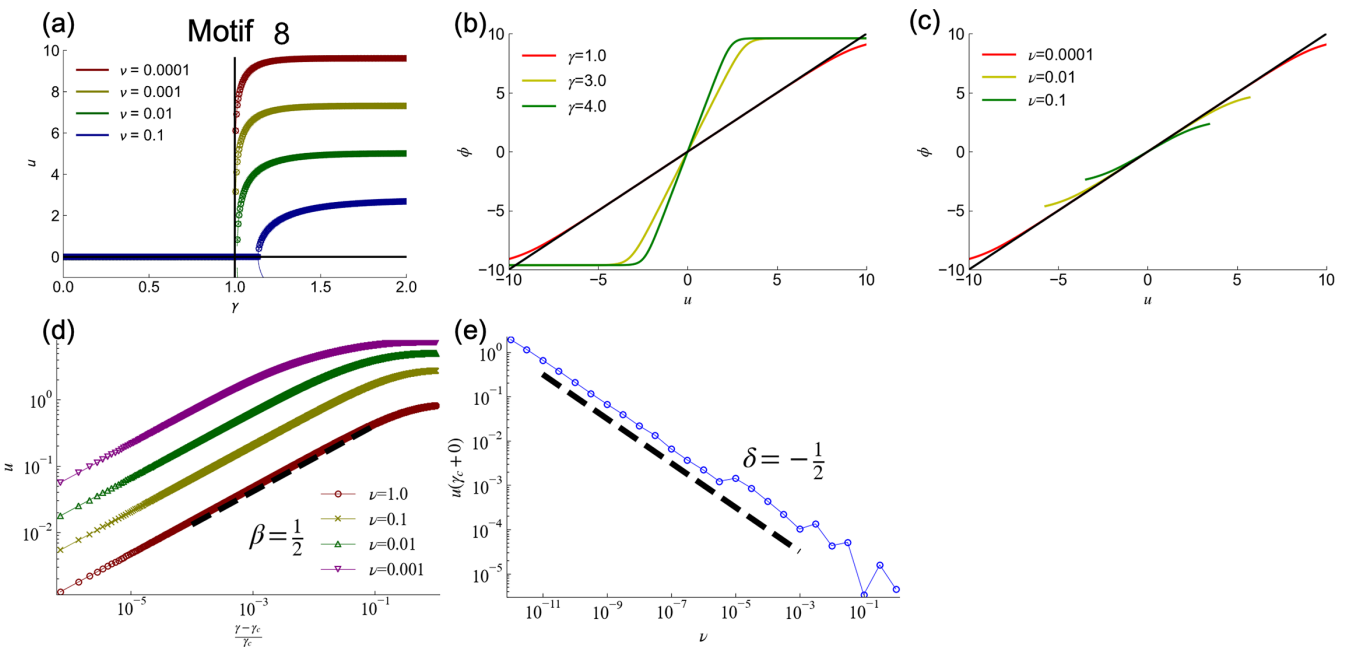

FIG. 4. Bifurcation analysis on motif 8. (a) The solution of Eq. (7) for $\nu = 10^{-4}$ (red), 10^{-3} (yellow), 10^{-2} (green), and 10^{-1} (blue). Points are the results obtained by numerically calculated stationary solution. Lines are the results based on Eq. (7); the black line indicates the solution of the self-consistency equation (7) at $\nu \to 0$. (b) The curves of the right-hand side ϕ of Eq. (7) at $\nu = 10^{-2}$ for $\gamma = 1.0$ (red), 2.0 (yellow), and 2.0 (green). The intersecting point with curves and the black line indicating $u = \phi$ corresponds to the stationary solution. The change of the number of intersecting points corresponds to the bifurcation. (c) The curves of the right-hand side ϕ of Eq. (7) at $\gamma = \gamma_c = 1 + \frac{2+\nu}{3+\nu}\nu$ for $\nu = 10^{-4}$ (red), 10^{-2} (yellow), and 10^{-1} (green). This figure implies that. (d) The scaling relationship of Eq. (13a) obtained by solving Eq. (7) numerically. The black line indicates the theoretical prediction of Eq. (18). (e) The scaling relationship of Eq. (13b) obtained by solving Eq. (7) numerically. The black line indicates the theoretical prediction of Eq. (22).

Figs. 3(a) and 4(a). To evaluate this quantitatively, we derive the exponents β and δ defined by

$$u \sim \left(\frac{\gamma - \gamma_c}{\gamma_c}\right)^{\beta}, \tag{13a}$$

$$u \sim \nu^{-\delta}, \tag{13b}$$

using Eq. (7). First, we expand the function ϕ up to third order:

$$u = \phi(u, \nu) = \frac{\gamma}{\gamma_c} u - \frac{x_0 + 1}{3(x_0 + 2)^2}(\gamma u)^3 + O(u^5), \tag{14}$$

or equivalently, if we ignore the higher-order term $O(u^5)$,

$$\left(1 - \frac{\gamma}{\gamma_c}\right)u + \frac{x_0 + 1}{3x_0^2}\left(\frac{\gamma}{\gamma_c}u\right)^3 = 0. \tag{15}$$

To derive the exponents β and δ, we set $\gamma = \gamma_c + \Delta\gamma$ with sufficiently small $\Delta\gamma > 0$ in Eq. (15) such that

$$\frac{\Delta\gamma}{\gamma_c}u - \frac{x_0 + 1}{3x_0^2}\left[\left(1 + \frac{\Delta\gamma}{\gamma_c}\right)u\right]^3 = 0. \tag{16}$$

Assuming $u \neq 0$ at $\gamma = \gamma_c + \Delta\gamma$, we have

$$\begin{aligned} u &= \left(\frac{3x_0}{x_0 + 1}\frac{\Delta\gamma}{\gamma_c}\right)^{\frac{1}{2}} + O(\Delta\gamma) \\ &= \left(\frac{3x_0^2}{(x_0 + 1)(x_0 + 2)}\Delta\gamma\right)^{\frac{1}{2}} + O(\Delta\gamma). \end{aligned} \tag{17}$$

Then, it is obvious that

$$u \sim \left(\frac{\gamma - \gamma_c}{\gamma_c}\right)^{\beta}, \ \beta = \frac{1}{2}. \tag{18}$$

This result is independent of the value of x_0, so both motifs 1 and 8 show the same scaling with the same β. This is natural because ϕ is an odd function. In the case of motif 1,

$$\begin{aligned} u &= \left(\frac{3\left(\frac{1}{1+\nu}\right)^3}{\left(\frac{1}{1+\nu} + 1\right)\left(\frac{1}{1+\nu} + 2\right)}\Delta\gamma\right)^{\frac{1}{2}} \\ &= \left(\frac{3}{(2 + \nu)(3 + 2\nu)(1 + \nu)}\Delta\gamma\right)^{\frac{1}{2}}. \end{aligned} \tag{19}$$

If we fix sufficiently small $\Delta\gamma$, then the dependency of ν on u is

$$u \sim \begin{cases} \text{constant}, & \text{if } \nu \ll 1, \\ \nu^{-\delta}, \ \delta = \frac{3}{2} & \text{if } \nu \gg 1. \end{cases} \tag{20}$$

In the same way, as in motif 1, we obtain

$$\begin{aligned} u &= \left(\frac{3\left(\frac{3+\nu}{\nu(2+\nu)}\right)^3}{\left(\frac{3+\nu}{\nu(2+\nu)} + 1\right)\left(\frac{3+\nu}{\nu(2+\nu)} + 2\right)}\Delta\gamma\right)^{\frac{1}{2}} \\ &= \left(\frac{3(3 + \nu)^3}{\nu(2 + \nu)(3 + 2\nu)(1 + \nu)(3 + 3\nu + \nu^2)}\Delta\gamma\right)^{\frac{1}{2}}. \end{aligned} \tag{21}$$

Hence, if we fix $\Delta\gamma$, we have

$$u \sim \nu^{-\delta}, \ \begin{cases} \delta = \frac{1}{2} & \text{if } \nu \ll 1, \\ \delta = \frac{3}{2} & \text{if } \nu \gg 1. \end{cases} \tag{22}$$

These scaling relations found in motifs 1 and 8 are confirmed numerically in Figs. 3(d), 3(e), 4(d), and 4(e) for sufficiently small ν. The scaling relation of Eq. (22) indicates that the localized solution of motif 8 does not exist at the zero-dissipation limit. This bifurcation is discontinuous at the zero-dissipation limit, and the crossover from the second-order transition to the first-order transition at $\nu > 0$ is observed.

The difference in the continuity of the bifurcation between motifs 1 and 8 at sufficiently small ν is due to positive feedback by reciprocal edges between node 0 and nodes 1 and 2. Motif 8 contains a feedback mechanism, which allows a flow between nodes 1 and 2 via node 0. Motif 1 does not contain such a feedback mechanism, so the flow between nodes 1 and 2 is absent and only dissipates outside. For sufficiently large ν, the continuity of bifurcation on motifs 1 and 8 is the same because the external dissipation becomes dominant and the feedback mechanism does not work.

B. Motif 13

In the case of motif 13, it is nontrivial from its structural symmetry whether the stationary solution can be captured by the single-order parameter $u = \ln \frac{x_2}{x_1}$. To verify that at least two of the three values of the stationary solution coincide, we calculate the vector field using the dynamics on the plane representing the conservation $x_0 + x_1 + x_2 = \frac{3}{\nu}$, which is given by

$$\begin{aligned} \frac{dx_0}{dt} &= \frac{x_0^\gamma}{x_2^\gamma + x_0^\gamma}x_1 + \frac{x_0^\gamma}{x_0^\gamma + x_1^\gamma}x_2 - (1 + \nu)x_0 + 1, \\ \frac{dx_1}{dt} &= \frac{x_1^\gamma}{x_0^\gamma + x_1^\gamma}x_2 + \frac{x_1^\gamma}{x_1^\gamma + x_2^\gamma}x_0 - (1 + \nu)x_1 + 1, \\ \frac{dx_2}{dt} &= \frac{x_2^\gamma}{x_1^\gamma + x_2^\gamma}x_0 + \frac{x_2^\gamma}{x_2^\gamma + x_0^\gamma}x_1 - (1 + \nu)x_2 + 1. \end{aligned} \tag{23}$$

Figures 5(b) and 5(c) show the vector fields of the right-hand side of Eq. (23) for $\gamma \leqslant \gamma_c^{(d)}$ for $\gamma = 0$ and 1. In these cases, the uniform solution $(\frac{1}{\nu}, \frac{1}{\nu}, \frac{1}{\nu})$ is the unique fixed point. This point is stable, and the vector field seems to flow into this fixed point. $\gamma = 1.5$ is shown in Fig. 5(d) as a typical case when $\gamma_c^{(d)} \leqslant \gamma \leqslant \gamma_c^{(u)}$. In this case, there exist three stable fixed points of the vector field, reflecting the symmetry in addition to the uniform solution, and there are also three unstable fixed points. In this case, stable fixed points other than the uniform solution observed in Fig. 5(d) still exist, and a transcritical bifurcation occurs where the stability of the uniform solution alternates with the unstable fixed points that existed in Fig. 5(d). As a result, in Fig. 5(f) for $\gamma = 2.5$ satisfying $\gamma \geqslant \gamma_c^{(u)}$, it is observed that the uniform solution becomes unstable and there are six stable fixed points in total. The three fixed points near the uniform solution correspond to the stationary solution obtained in Fig. 2(c), and the three fixed points at the edge of the triangle correspond to the stationary solution obtained in Fig. 2(d). From Figs. 5(b)–5(f), it is confirmed that fixed points exist only when at least two of three coincide in all cases. Therefore, by observing the behavior of $u = \ln \frac{x_2}{x_1}$, we can analyze the bifurcation phenomenon and find that it does not lose its generality. To confirm the nonexistence

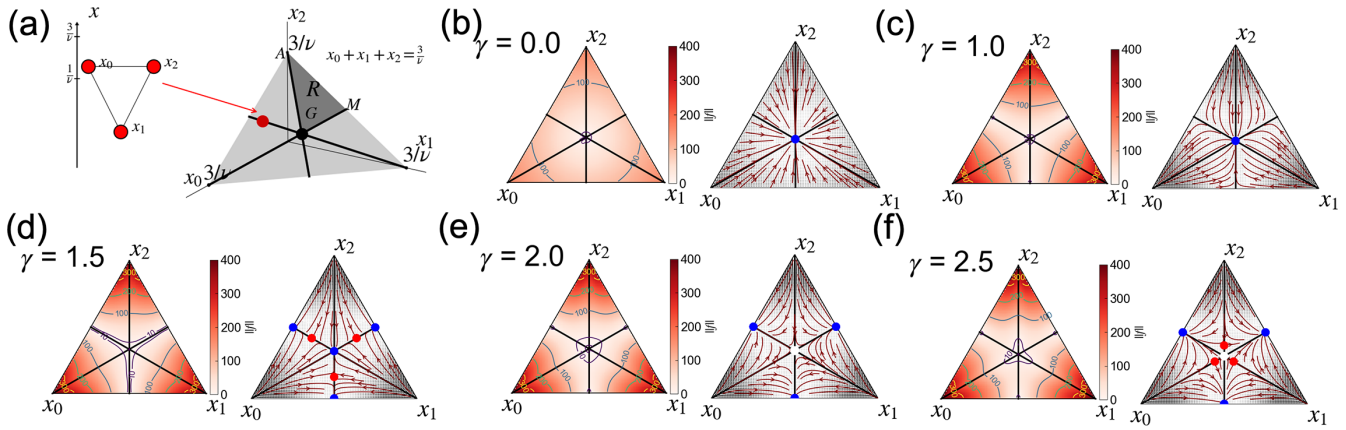

FIG. 5. Streamlines of the vector fields given by the right-hand side of Eq. (23) on the plain representing the conservation law $x_0 + x_1 + x_2 = \frac{3}{\nu}$ for $\gamma = 0$, 1, 1.5, 2, 2.5, and 3. In panels (b)–(f), the fixed points are annotated by points, the blue points correspond to stable fixed points, the red points correspond to saddle points, and the white points correspond to unstable fixed points. (a) The mapping to the phase diagram on the triangle $x_0 + x_1 + x_2 = \frac{3}{\nu}$. The point G on the right side is the point representing the uniform solution $(\frac{1}{\nu}, \frac{1}{\nu}, \frac{1}{\nu})$. The red point represents the state (x_0, x_1, x_2) corresponding to the left side. The highlighted triangle region R corresponds to the subset of phase space such that $x_0 < x_1 < x_2$. (b) $\gamma = 0$. Streamlines are flowing into the unique fixed point G. (c) $\gamma = 1.0$. Streamlines are flowing into unique fixed point G, as in the case of panel (b). (d) $\gamma = 1.5$. This case satisfies $\gamma_c^{(d)} \leqslant \gamma \leqslant \gamma_c^{(u)}$. There are multiple stable fixed points other than the uniform solution G. (e) $\gamma = 2.0$. The transcritical bifurcation where the stability of the unstable fixed points and the stable fixed point G change. (f) $\gamma = 2.5$. The fixed point G is unstable, and multiple stable fixed points corresponding to two localized states in Figs. 2(c) and 2(d) are present.

of the periodic solution, we focus on the vector field in the region R corresponding to the set $\{(x_0, x_1, x_2) | x_0 < x_1 < x_2\}$ without loss of generality [see Fig. 5(a) for visualization]. In the case of $\gamma < \gamma_c^{(\mathrm{d})}$, the vector field in R flows into the blue point corresponding to the uniform solution. In the case of $\gamma_c^{(\mathrm{d})} < \gamma < \gamma_c^{(\mathrm{u})}$, the vector field in R flows into the edge GM. In the case of $\gamma > \gamma_c^{(\mathrm{u})}$, the vector field in R flows into the blue point corresponding to the localized stable solution. In any case, the vector field does not have any fixed points in the interior of R, and there must not exist periodic solutions since the vector field is gradientlike, due to Bendixson's theorem [27]. Finally, there are no periodic solutions across the region R since the region R does not have vector fields crossing boundaries. This completes the intuitive argument.

By setting $x_0 = x_2$, we define the order parameter $u = \ln \frac{x_2}{x_1}$ of localization of the stationary solution. The self-consistency equation is then

$$u = \phi(u, \gamma, \nu) = \frac{1 + \nu}{\frac{2}{1+u^\gamma} + \frac{\nu}{3}\left(2 + \frac{1}{u}\right)}. \tag{24}$$

By finding the solution of Eq. (24), we obtain Fig. 6(a). In Fig. 6(a), the markers are obtained by numerical calculation of the model, and the solid line is the solution of Eq. (24). From this figure, we can see a saddle-node bifurcation at $\gamma = \gamma_c^{(d)}$ and a transcritical bifurcation at $\gamma = \gamma_c^{(u)}$. There are two stable fixed points in $\gamma \geqslant \gamma_c^{(u)}$, and they are consistent with the existence of two different stationary solutions in motif 13, as obtained in Figs. 2(c) and 2(d). The behavior of the right-hand side of Eq. (24) is shown in Figs. 6(b) and 6(c). At $\gamma = \gamma_c^{(d)}$, a pair of stable and unstable fixed points different from the uniform solution appears, and at $\gamma = \gamma_c^{(u)}$, the stability of the unstable fixed point and uniform solution change.

To proceed, we rewrite the equation with respect to γ as follows:

$$\gamma = \psi(u, \nu) \equiv \frac{1}{u} \ln \frac{e^u/a - 1}{1 - be^u},$$
$$a = \frac{\frac{2}{3}\nu + 1}{\frac{2}{3}\nu + 2}, \quad b = \frac{\frac{2}{3}\nu}{\frac{2}{3}\nu + 1}. \tag{25}$$

The motif of the function ψ is shown in Fig. 6(c). Laurent expansion of ψ at $u = 0$ is

$$\begin{aligned}\gamma = \psi(u, \nu) &= \frac{1 - ab}{(1-a)(1-b)} - \frac{(1-ab)(a-b)}{2(1-a)^2(1-b)^2}u \\ &\quad + O(u^2) \\ &= \gamma_c^{(13u)} - \frac{1}{2}\gamma_c^{(13u)}u + O(u^2), \\ \gamma_c^{(13u)} &= 2 + \frac{4}{3}\nu. \end{aligned} \tag{26}$$

This proves the scaling relationship of continuous bifurcation in Fig. 2(c):

$$u \sim \left(\frac{\gamma - \gamma_c}{\gamma_c}\right)^\beta, \ \beta = 1. \tag{27}$$

The bifurcation point $\gamma_c^{(13d)}$ where a two-point localized solution discontinuously jumps to the uniform solution is obtained as the minimum of $\psi(u, \nu)$:

$$\gamma_c^{(13d)}(\nu) = \min_u \psi(u, \nu). \tag{28}$$

The bifurcation point $\gamma_c^{(13d)}$ is obtained numerically by solving Eq. (28) in Fig. 6(f). We found that $\gamma_c^{(13d)}$ slowly converges to 1 from the upper side. To consider $\nu \to 0$, we

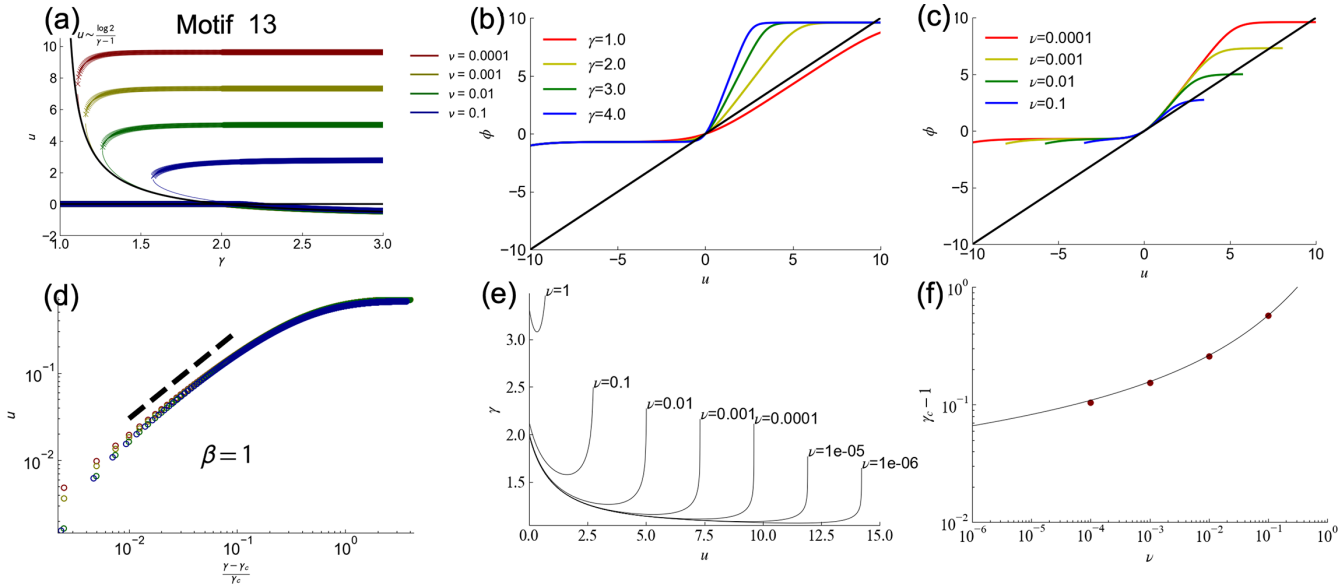

FIG. 6. Bifurcation analysis on motif 13. (a) The solution of Eq. (24) for $\nu = 10^{-4}$ (red), 10^{-3} (yellow), 10^{-2} (green), and 10^{-1} (blue). Points are the results obtained by the numerically calculated stationary solution. Lines are the results based on Eq. (24); the black line indicates the solution of the self-consistency equation (24) at $\nu \to 0$. (b) The curves of the right-hand side ϕ of Eq. (24) at $\nu = 10^{-2}$ for $\gamma = 1.0$ (red), 2.0 (yellow), and 2.0 (green). (c) The curves of the right-hand side ϕ of Eq. (24) at $\gamma = \gamma_c = 1 + \frac{2+\nu}{3+\nu}\nu$ for $\nu = 10^{-4}$ (red), 10^{-2} (yellow), and 10^{-1} (green). (d) The scaling relation of Eq. (27). The simulation result is presented by red ($\nu = 10^{-4}$), yellow ($\nu = 10^{-3}$), green ($\nu = 10^{-2}$), and blue ($\nu = 10^{-1}$) points. The black line is the theoretical prediction. (e) The right-hand side of Eq. (25). The values at $u = 0$ of curves are $\gamma_c^{(u)}$. For sufficiently small ν, $\gamma_c^{(u)}$ is approximately 2, which is consistent with Eq. (26). The minima of the curves are $\gamma_c^{(d)}$. For sufficiently small ν, $\gamma_c^{(d)}$ is asymptotically close to 1, which is consistent with Eq. (30). (f) The asymptotics of $\gamma_c^{(d)}$. The red points are obtained by numerical simulation of Eq. (23), and the black line is the curve of Eq. (28).

approximate that $a = \frac{1}{2}$ and $b = 0$ in Eqs. (25) to obtain

$$\gamma - 1 = \frac{\ln 2}{u} + \frac{1}{2}\frac{e^{-u}}{u}. \tag{29}$$

From this relation, at the limit $\nu \to 0$, we found that

$$\gamma_c^{(d)} \to 1 \tag{30}$$

because $u \to \infty$.

IV. DISCUSSION

In this study, we investigated the bifurcation on three classes of network motifs with three nodes, i.e., motifs 1, 8, and 13 in Fig. 1(c), and we found that the bifurcation points of these three motifs are different, and the type of bifurcation changes from supercritical pitchfork to a combination of the saddle-node and transcritical bifurcation by adding edges to the motif. Furthermore, we found that hysteresis loops are

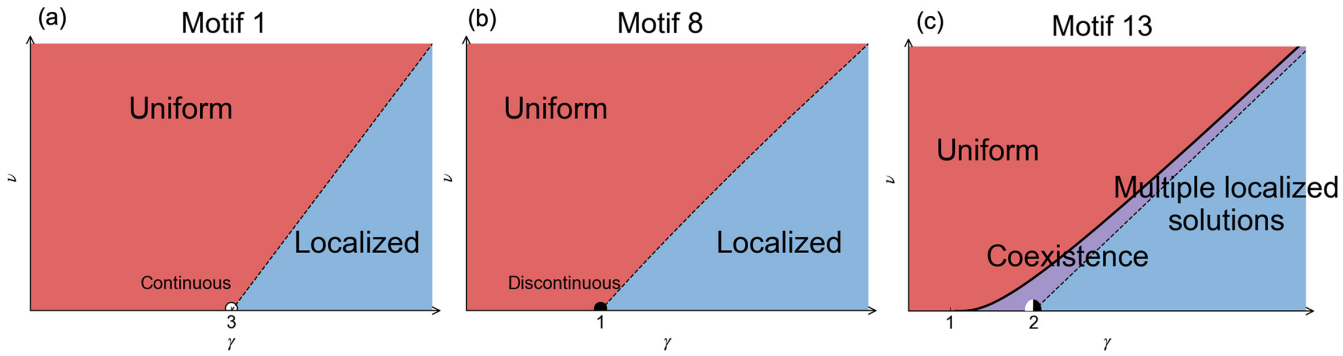

FIG. 7. Phase diagram of the model on motifs (a) 1, (b) 8, and (c) 13. Red areas in panels (a)–(c) indicate areas where uniform solutions are stable; blue areas in panels (a)–(c) indicate areas where uniform solutions become unstable and localized solutions are stable; and the purple area in panel (c) indicates areas where stable uniform solutions and stable and saddle localized solutions coexist, respectively. In the blue area in panel (c), motif 13 has multiple stable solutions and multiple saddle solutions due to the symmetry of three nodes. As the boundaries of the areas, dotted lines in the figure represent Eqs. (4a) (motif 1), (4b) (motif 8), and (4c) (motif 13), and the solid black line in panel (c) represents Eq. (28). The circles on the x axis indicate the destabilization of the uniform solution: (a) the solution bifurcates continuously (represented by a white marker), (b) it bifurcates discontinuously (represented by a black marker), and (c) both continuous and discontinuous bifurcations exist simultaneously (represented by a black and white dual-half marker), corresponding to Figs. 2(c) and 2(d).

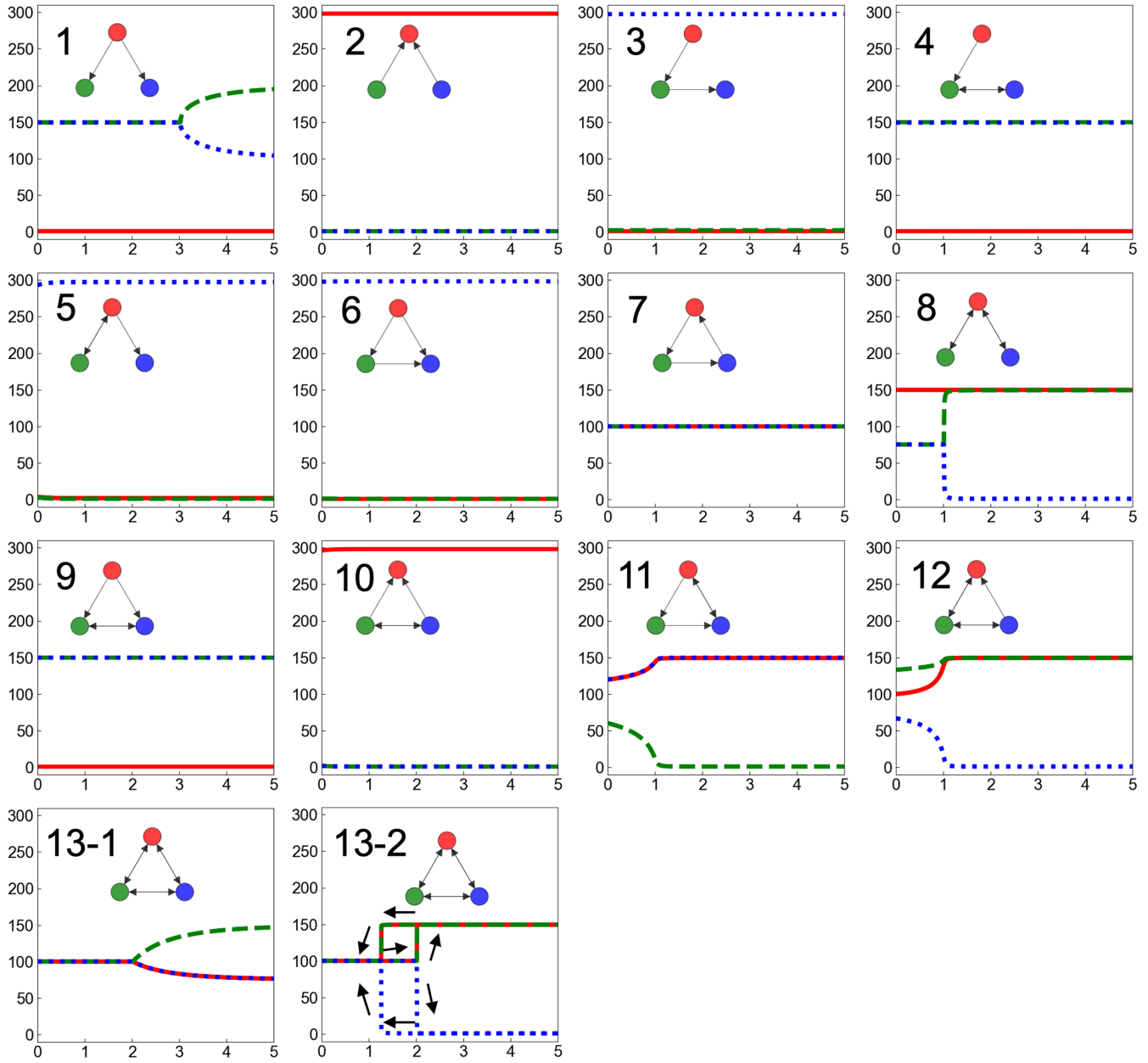

FIG. 8. Numerical simulation results obtained for all 13 network motifs with three nodes. The number of each panel corresponds to the motif identification number. As mentioned in the main text, motif 13 shows different bifurcation patterns depending on the perturbation (see panels 13-1 and 13-2). For each panel, the horizontal axis is the control parameter γ, and the vertical axis is the value of the stationary solution x. Only three motifs, motifs 1, 8, and 13, exhibit bifurcation in $0 \leqslant \gamma \leqslant 5$ with $\nu = 0.01$. The reasons why the other ten motifs do not exhibit bifurcation are classified into several categories. Motifs 2, 3, 4, and 7 do not have branching nodes, i.e., nodes with the outdegree being greater than or equal to 2; thus, the stationary solution is independent of γ. Motifs 5, 6, and 10 have one sink node (the blue node in motifs 5 and 6, and the red node in motif 10); thus, the stationary solution is already localized at $\gamma = 0$. Motif 9 has a symmetry of green and blue nodes, and in fact, it exhibits bifurcation at a large bifurcation point. The bifurcation point goes to infinity at $\nu \to 0$ because the bidirectional edge between the green and blue nodes helps to converge faster to the stationary state.

created between 1 and 2 in the case of motif 13. These results are summarized in phase diagrams [Figs. 7(a)–7(c)]. The diagrams show the stable solution at given (γ, ν) values. In the case of motifs 1 and 8, there are only two parameter regions where uniform or localized solutions are stable. However, in the case of motif 13, there is a parameter region of coexistence of uniform and localized solutions other than regions corresponding to uniform or localized stable solutions.

Various models of the nonlinear transport and the interaction of size variables have been proposed and analyzed to date. The multistability of some of the models was known, but its origin was not clear, as a previous paper pointed out [13]. It is expected that the study of the models on the three-body system may give a better understanding of the mechanism, and we hope that the relation between the bifurcation and hysteresis we showed alongside previously reported results will be clarified in the near future.

As we found the hysteresis of the model on small-size networks, we may potentially observe a hysteresis on other real systems with small-size networks, such as international trade and human flow between cities in the long run. The role of the hysteresis of this nonlinear transport model may be associated with the stability of many social economic systems.

Only a few studies have directly discussed the modeling of nonlinear transport and system stability in complex networks with hundreds to millions of degrees of freedom, which are assumed to be realistic systems. In the nonlinear transport model we studied, our results may be associated with the phase transitions on the Japanese business network [17], which is known to be scale-free and small-world, and hysteresis [20] on a certain scale-free network generation model [28]. It is suggested that motif 13 plays the role of bistable elements in a large-degree-of-freedom system. Although our results were obtained for three systems, they are expected to be essential for explaining the bifurcation phenomena in large-degree-of-freedom systems obtained to date, as it is known that the number of motif 13 is significant by the network motif analysis of the Japanese business network [29,30]. However, the problem remains that many of the bifurcation points of the large networks are less than 1, as in the case of the Japanese business network [17], which is different from the bifurcation points obtained in the three-body system.

For future work, it is desired to investigate bifurcation in large-scale networks, such as the Japanese business network, as a phase transition using our results to clarify the universality of the diffusion-localization phase transition in large-scale networks. There is a possibility that the transition point γ_c and critical behavior of the transition can be determined by only the degree distribution. It is expected that the answer to these fundamental questions may contribute to our understanding of the behavior of nonlinear transport and eventually to the stability of many real systems.

ACKNOWLEDGMENTS

This work is supported by Japan Society for the Promotion of Science KAKENHI Grant No. 23KJ0921. This work has received financial support from Tokyo Institute of Technology collaborative chair of Teikoku Databank, Ltd. H.K. was financially supported by the Japan Society for the Promotion of Science, Research Fellowship for Young Scientists. H.K. designed the study, performed the numerical experiments, interpreted the results, developed the theoretical analysis, and wrote the manuscript. H.T. designed the study, interpreted the results, and revised the manuscript. M.T. directed the study, designed the study, interpreted the results, and revised the manuscript.

APPENDIX: NUMERICAL RESULTS ON ALL 13 NETWORK MOTIFS

In this section, we show the bifurcation diagrams for all 13 network motifs with three nodes obtained by the procedure described in the main text (see Fig. 1 for an overview of the procedure). The resulting figures are presented in Fig. 8.

We add some remarks on why ten motifs do not show bifurcation. First, it is obvious that motifs 2, 3, 4, and 7 do not exhibit bifurcation because these motifs do not have branching nodes, i.e., nodes with the outdegree being greater than or equal to 2. For simplicity, here, we discuss the differences between motifs 6 and 9, and motif 1. Motif 1 has a symmetry of green and blue nodes, but motif 6 has one direct edge from the green node to the blue node. This edge breaks the symmetry between green and blue nodes, leading to a drastic change in the stationary solution of the model. The stationary solution at $\gamma = 0$ is concentrated on the blue node, which is the only sink of the motif. This implies that there is no drastic change of stationary solution by controlling γ, which is why motif 6 does not exhibit bifurcation at all, as in Fig. 8(6). This reasoning for motif 6 also applies to motifs 5 and 10. Meanwhile, motif 9 has a different reason that bifurcation does not occur at $\nu \to 0$. This motif actually bifurcates at some γ_c, and we can show that $\gamma_c \to \infty$ as $\nu \to 0$. The bifurcation point is determined by the ratio of the decay rate $2 + \nu$ of the perturbation by the dissipation rate ν as

$$\text{motif 9: } \gamma_c = (3 + 2\nu)\frac{2 + \nu}{\nu} \geqslant 7 + 4\sqrt{3} \approx 14 (\nu = \sqrt{3}). \tag{A1}$$

The interaction between green and blue nodes is very fast compared to the external dissipation. As the slowest dynamics dominate at the long-time behavior, the large value of γ is needed to bring about bifurcation. This implies that if the external dissipation is sufficiently small, the bifurcation point is very high according to Eq. (A1). As a result, no bifurcation happens at $0 \leqslant \gamma \leqslant 5$ with $\nu = 0.01$ in Fig. 8 (motif 9).

[1] J. Tinbergen, Shaping the world economy, Int. Exe. **5**, 27 (1963).
[2] E. G. Ravenstein, The laws of migration, J. R. Stat. Soc. **52**, 241 (1889).
[3] G. K. Zipf, The P_1P_2/D hypothesis: On the intercity movement of persons, Am. Sociological Rev. **11**, 677 (1946).
[4] J. J. Lewer and H. Van den Berg, A gravity model of immigration, Econ. Lett. **99**, 164 (2008).
[5] G. Krings, F. Calabrese, C. Ratti, and V. D. Blondel, Urban gravity: a model for inter-city telecommunication flows, J. Stat. Mech.: Theory Exp. (2009) L07003.
[6] H. J. Park, W. S. Jo, S. H. Lee, and B. J. Kim, Generalized gravity model for human migration, New J. Phys. **20**, 093018 (2018).
[7] R. Prieto Curiel, L. Pappalardo, L. Gabrielli, and S. R. Bishop, Gravity and scaling laws of city to city migration, PLoS ONE **13**, e0199892 (2018).
[8] A. P. Masucci, J. Serras, A. Johansson, and M. Batty, Gravity versus radiation models: On the importance of scale and heterogeneity in commuting flows, Phys. Rev. E **88**, 022812 (2013).
[9] W.-S. Jung, F. Wang, and H. E. Stanley, Gravity model in the Korean highway, Europhys. Lett. **81**, 48005 (2008).

[10] R. Li, S. Gao, A. Luo, Q. Yao, B. Chen, F. Shang, R. Jiang, and H. E. Stanley, Gravity model in dockless bike-sharing systems within cities, Phys. Rev. E **103**, 012312 (2021).
[11] J. E. Anderson, The gravity model, Annu. Rev. Econ. **3**, 133 (2011).
[12] K. Tamura, W. Miura, M. Takayasu, H. Takayasu, S. Kitajima, and H. Goto, Estimation of flux between interacting nodes on huge inter-firm networks, Int. J. Mod. Phys.: Conf. Ser. **16**, 93 (2012).
[13] P. S. Skardal and S. Adhikari, Dynamics of nonlinear random walks on complex networks, J. Nonlinear Sci. **29**, 1419 (2019).
[14] P. S. Skardal, Quasiperiodic dynamics and a Neimark-Sacker bifurcation in nonlinear random walks on complex networks, Phys. Rev. E **101**, 012307 (2020).
[15] D. Chitrakar and P. S. Skardal, Chaos in nonlinear random walks with nonmonotonic transition probabilities, Phys. Rev. Res. **3**, 043189 (2021).
[16] P. S. Skardal, Pattern formation and oscillations in nonlinear random walks on networks, arXiv:2211.12602.
[17] K. Tamura, H. Takayasu, and M. Takayasu, Diffusion-localization transition caused by nonlinear transport on complex networks, Sci. Rep. **8**, 5517 (2018).
[18] H. Koike, H. Takayasu, and M. Takayasu, Diffusion-localization transition point of gravity type transport model on regular ring lattices and Bethe lattices, J. Stat. Phys. **186**, 44 (2022).
[19] C. Falcó, From random walks on networks to nonlinear diffusion, Phys. Rev. E **106**, 054103 (2022).
[20] J. Ozaki, K. Tamura, H. Takayasu, and M. Takayasu, Modeling and simulation of Japanese inter-firm network, Artif. Life Rob. **24**, 257 (2019).
[21] F. Horn and R. Jackson, General mass action kinetics, Arch. Ration. Mech. Anal. **47**, 81 (1972).
[22] M. Newman, A.-L. Barabási, and D. J. Watts, *The Structure and Dynamics of Networks* (Princeton University, Princeton, NJ, 2011).
[23] M. Newman, *Networks* (Oxford University, Oxford, 2018).
[24] A. Barrat, M. Barthelemy, and A. Vespignani, *Dynamical Processes on Complex Networks* (Cambridge University, Cambridge, England, 2008).
[25] R. Milo, S. Shen-Orr, S. Itzkovitz, N. Kashtan, D. Chklovskii, and U. Alon, Network motifs: simple building blocks of complex networks, Science **298**, 824 (2002).
[26] U. Alon, Network motifs: theory and experimental approaches, Nat. Rev. Genet. **8**, 450 (2007).
[27] J. Guckenheimer and P. Holmes, *Nonlinear Oscillations, Dynamical Systems, and Bifurcations of Vector Fields*, Applied Mathematical Sciences Vol. 42 (Springer, New York, 2013).
[28] W. Miura, H. Takayasu, and M. Takayasu, Effect of coagulation of nodes in an evolving complex network, Phys. Rev. Lett. **108**, 168701 (2012).
[29] T. Ohnishi, H. Takayasu, and M. Takayasu, Network motifs in an inter-firm network, J. Econ. Interact. Coord. **5**, 171 (2010).
[30] J. Maluck, R. V. Donner, H. Takayasu, and M. Takayasu, Motif formation and industry specific topologies in the Japanese business firm network, J. Stat. Mech.: Theory Exp. (2017) 053404.